

Vision-based technique for bolt-loosening detection in wind turbine tower

Jae-Hyung Park^a, Thanh-Canh Huynh^b, Sang-Hoon Choi^c and Jeong-Tae Kim^{*}

Department of Ocean Engineering, Pukyong National University, 45 Yongso-ro, Nam-gu, Busan, Korea

(Received November 3, 2015, Revised November 30, 2015, Accepted December 2, 2015)

Abstract. In this study, a novel vision-based bolt-loosening monitoring technique is proposed for bolted joints connecting tubular steel segments of the wind turbine tower (WTT) structure. Firstly, a bolt-loosening detection algorithm based on image processing techniques is developed. The algorithm consists of five steps: image acquisition, segmentation of each nut, line detection of each nut, nut angle estimation, and bolt-loosening detection. Secondly, experimental tests are conducted on a lab-scale bolted joint model under various bolt-loosening scenarios. The bolted joint model, which is consisted of a ring flange and 32 sets of bolt and nut, is used for simulating the real bolted joint connecting steel tower segments in the WTT. Finally, the feasibility of the proposed vision-based technique is evaluated by bolt-loosening monitoring in the lab-scale bolted joint model.

Keywords: bolted joint; bolt loosening; vision; image processing; steel structure; wind turbine tower

1. Introduction

Wind energy has been regarded as a strong contender among renewable power sources due to its reliability and relative cost effectiveness. In the recent years, the needs of higher efficiency in wind energy harvesting and cost competitiveness have led to the increment in the size of wind turbines (Ciang *et al.* 2008). Steel wind turbines are normally pre-fabricated in factories and assembled in the field via in-situ structural joints. Due to the convenience in installation and the ability to carry tension loads, axially preloaded bolted joints are designed for various types of in-situ connections of wind turbine structures. Besides connecting tower segments, preloaded bolts are also used for joints between nacelle and blade, or for the machineries. Insufficient or excessive preloading for the joints are considered as major causes of the joint failure. Therefore, to provide the safety for wind turbine structures and the reliability for power generation, the high-tension bolted joints should be appropriately monitored to ensure their healthy conditions (Basava and Hess 1998, Izumi *et al.* 2005, Wang *et al.* 2013a).

Many bolt-loosening monitoring methods have been developed for indirectly measuring bolt

*Corresponding author, Professor, E-mail: idis@pknu.ac.kr

^a Ph.D., E-mail: cross96@gmail.com

^b Graduate Student, E-mail: ce.huynh@gmail.com

^c Graduate Student, E-mail: skgodsus@gmail.com

tension so far (Wang *et al.* 2013a). The loss of bolt's preload could be identified by using nondestructive techniques such as: the guided wave method, impedance method, the magnet field method, and the electric potential drop method. The guided wave-based technique utilizes the change in the ultrasonic wave generated by the piezoelectric transducer, which is passing through the splice plate, to detect the bolt-loosening. The received ultrasonic wave is altered when the loss of bolt preload changes the dynamic characteristics of the splice plate (Park *et al.* 2006, Kim and Hong 2009, Wang *et al.* 2013b). The impedance-based method has high sensitivity to the local structural damage and the wide frequency bandwidth. It is specially fitted for monitoring bolted joints, which are dominated by local dynamics of high-frequency characteristics (Park *et al.* 2001, Kim *et al.* 2011, Ho *et al.* 2012, Huynh *et al.* 2015). The magnet field-based method is based on a simple phenomenon in which the bolt-loosening is caused by rotating a nut and this rotation changes magnetic field around the nut (You *et al.* 2010). The electric potential drop method uses the relationship between the electrical resistance and the change in thickness of a steel splice plate to alarm the bolt-loosening. If a bolt is loosened, the cross-section area of the splice plate is increased, making the electric resistance decreased (Hyun 2013).

Despite their potentials for bolt-loosening monitoring, the above-mentioned methods need high-cost data acquisition systems and also require a number of sensors to cover all bolts in a large-sized connection. In addition, changes in in-situ environmental conditions such as temperature variation could affect the accuracy of bolt-loosening detection since sensing materials used in these techniques are temperature-dependent. Hence, an alternative monitoring technique should be sought for in-situ health monitoring of large-scale bolted connections in wind tubular tower (WTT) structures.

Up-to-date, image processing techniques have been widely adopted to recognize medical images, objects, patterns, characters and so on. Many researchers have made their attempts to utilize the techniques for inspection and monitoring of civil structures. The techniques were used to identify cracks on concrete (Abdel-Qader *et al.* 2003, Hutchinson and Chen 2006, Yamaguchi and Hashimoto 2010) and pavement surface (Subirats *et al.* 2006, Zou *et al.* 2012), to detect and evaluate corrosion occurred in steel structures (Choi and Kim 2005, Lee *et al.* 2006, Korea Expressway Corporation 2006), to detect damage on the surface of stay cables in cable-stayed bridges (Ho *et al.* 2013), and to measure displacement of the bridge (Fukuda *et al.* 2013). The primary benefits of the image-based techniques for civil structures are as follows: (1) providing intuitive, quantitative, and temperature-free information for structure maintenance, (2) utilizing low-cost equipment such as cameras which are non-contact sensors, and (3) being able to inspect a large-sized area on structures by using only one camera.

By adopting these advantages, a novel vision-based bolt-loosening monitoring technique is proposed for bolted joints connecting tubular steel segments of the WTT structure. Firstly, a bolt-loosening detection algorithm, which is based on image processing techniques, is developed. The algorithm consists of five major steps: (1) acquiring the image from the bolt joint, (2) identifying all nuts in the image by segmenting the image for each nut by Canny edge detector and circular Hough transform, (3) identifying all lines of nuts by Hough transform, (4) estimating rotation angles of the identified nuts, and (5) detecting bolt-loosening occurrence of the change of the rotation angles estimated from the reference and current images. Secondly, experimental tests are conducted on a lab-scale bolted joint model under various bolt-loosening scenarios. The bolted joint model, which is consisted of a ring flange and 32 sets of bolt and nut, is used for simulating the real bolted joint connecting steel tower segments in the WTT. Finally, the feasibility of the proposed vision-based technique is evaluated by bolt-loosening monitoring in the lab-scale bolted

joint model.

2. Novel vision-based bolt-loosening monitoring technique

2.1 Vision-based bolt-loosening monitoring algorithm

A novel bolt-loosening detection technique using the image processing is particularly proposed for the bolted joints connecting steel tower segments of WTT structures. The fundamental concept of this technique is based on monitoring the change in rotational angles of nuts from the nut images acquired at different times. As compared to other nondestructive techniques, the vision-based technique is cost-efficient and able to quickly detect bolt-loosening since it requires only images of bolted joints.

As shown in Fig. 1, the proposed technique is outlined with five steps. In the first step, an image of a bolt joint in a steel WTT is acquired by a CCD (charge-coupled device) camera, the so-called digital camera. The camera should be fixed at the center of the cross-section of the tower with a proper object distance (L) to include all nuts in a photo, as plotted in Fig. 2. The minimum object distance L can be simply calculated as

$$L \geq \frac{h_{obj}}{h_s} d_f \tag{1}$$

where h_{obj} is the outer diameter of the cross-section of the tower, h_s is the height of the image sensor of the digital camera and d_f is the minimum focal length. The image of bolted joint is continuously captured within a long-term period because bolts are not loosened rapidly.

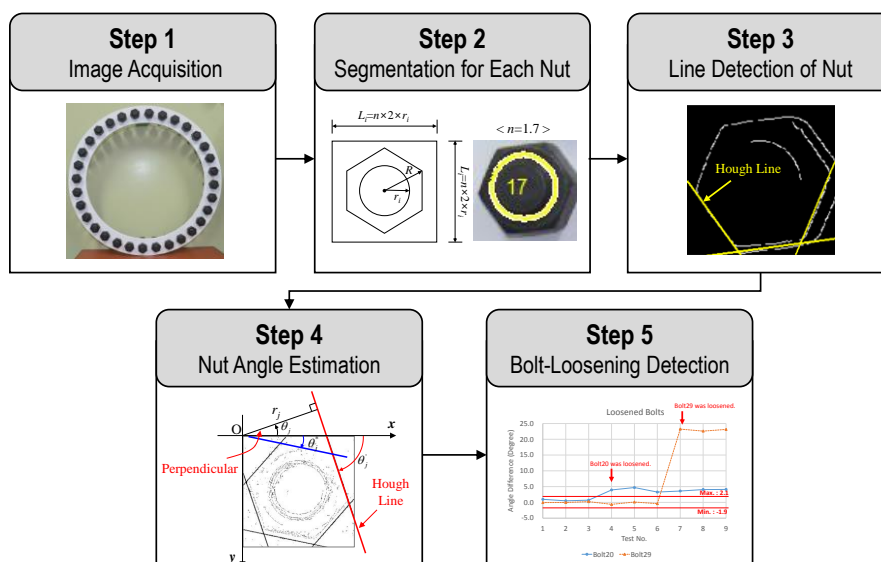


Fig. 1 Process of the vision-based bolt-loosening monitoring technique

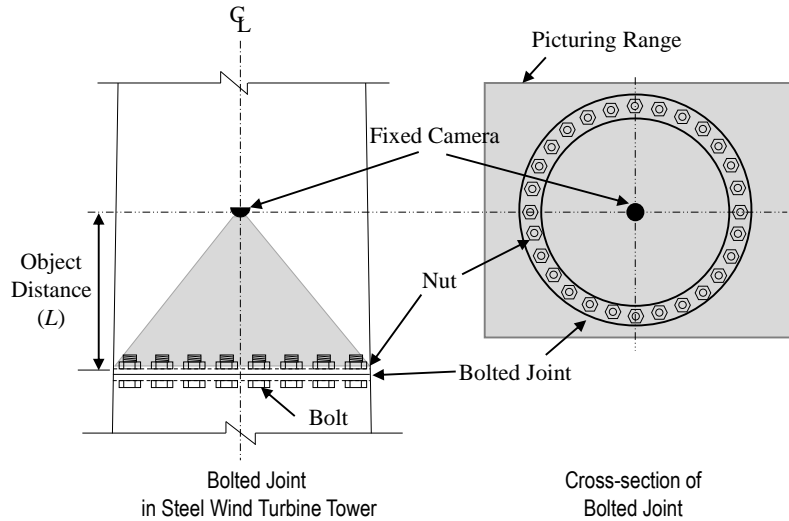


Fig. 2 Image acquisition schematic of the proposed technique for a bolted joint of a WTT

In the second step, each nut in the image is identified, and the image is segmented for each nut in order to detect bolt-loosening one by one. Firstly, the image is transformed to a gray scale image. Then, image edges are detected by the Canny edge detector. Next, circular shapes, which mean the bolt tips in the image, are detected from the edge image by using the circular Hough transform (CHT). (Note that the details of the Canny detector and the CHT are described in the following sub-sections 2.2 and 2.3). By using the information of the circles found by the CHT (i.e., center coordinates and radiuses), the image is segmented to sub-images for the all nuts as

$$L_i = n \times 2 \times r_i \quad (2)$$

where L_i is the size of the sub-image for the i^{th} nut, r_i is the identified radius of the i^{th} bolt tip, n is a ratio between the real radius of the bolt tip r_c and R , and R is distance between the center of the nut and a corner of the nut, as shown in the Fig. 3. In general, the n values for most pairs of bolt and nut have about 1.5 ~ 1.6. Considering the estimation error of r_c by the CHT, however, n should be selected to a larger value than the 1.6. Finally, the sub-images are labelled in the clockwise direction by using the center coordinates for each nut and the cross-section of the tower, as shown in Fig. 4. The center for the cross-section of the tower can be easily determined by averaging the center coordinates of all nut.

In the third step, the Hough transform (HT) is performed on the each sub-image including a nut to detect k lines, which could potentially represent the nut's edges. (Note that the details of the HT are described in the following sub-section 2.3). The detected lines correspond to six edges of the nut as well as unexpected lines by noises. Fig. 5(a) shows the unexpected lines passing through the bolt tip detected by the HT. Those unexpected lines can be easily eliminated by substituting the line equations (extracted by the HT) into the circle equation (estimated by the CHT) and checking their discriminants. Then, p strongest lines are selected as shown in the Fig. 5(b). The larger p is selected, the higher accuracy might be, and p cannot be larger than the number of edges of a nut (e.g., six for a hexagon).

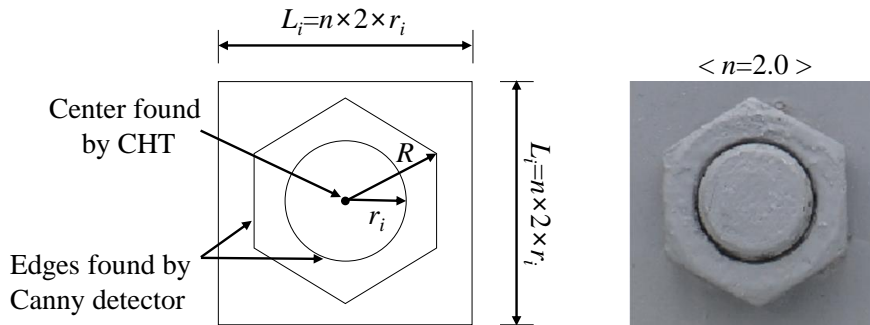


Fig. 3 An example of segmented image for a nut

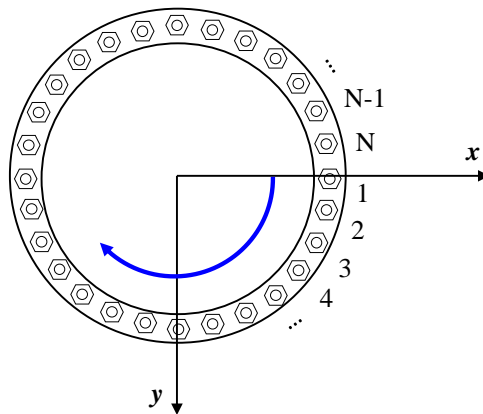


Fig. 4 Labelling the segmented images

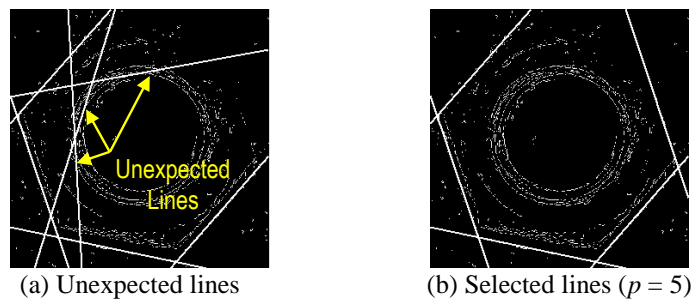


Fig. 5 An example for line detection from a nut image by HT

In the fourth step, the rotation angle θ'_j of the each nut is estimated, see Fig. 6, as follows

$$\theta'_j = 90 + \theta_j \tag{3}$$

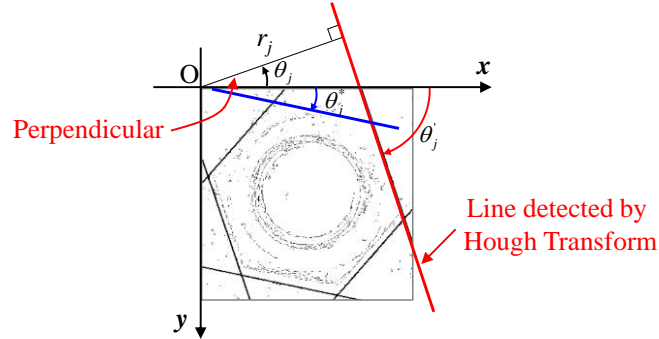


Fig. 6 Identified lines by the Hough transform and definition of the rotation angle of a nut

where θ_j is the angle for perpendicular of the j^{th} line detected by the HT. As shown in Fig. 6, the HT finds lines on an image by using distances r_j for perpendiculars from the origin to the lines and angles θ_j between the x-axis and the perpendiculars. For the consistency of angle estimation, the identified rotation angles can be expressed to ones in the range of 0 ~ 60 degrees due to the nut shape with a regular hexagon, as follows

$$\theta_j^* = \text{rem}[\theta_j' / 60] \quad (4)$$

where θ_j^* is the rotation angle in the range of 0 ~ 60 degrees for the j^{th} detected line as shown in Fig. 6 and $\text{rem}[\bullet]$ is an operator to calculate the remainder after division. Note that the rotation angle of a nut is recognized as the same one when the nut is rotated through every 60 degrees. Finally, the angle of nut is estimated by averaging the p angles in the range of 0 ~ 60 degrees.

In the final step, the bolt-loosening of the each nut is simply detected by comparing the initial and the current estimated angles. By considering the estimation error of the nut's angle, the bolt-loosening of each nut is alarmed if the difference between the initial and the current estimated angles is larger than the estimation error, as follows

$$|\Delta\theta_j^*| > \theta_e \quad (5)$$

where θ_e is the threshold value or criteria considering nut's angle estimation error of the proposed algorithm.

2.2 Canny edge detector

The Canny edge detector (Canny 1986) is one of commonly used edge detection methods based on gradient. Similar to the other gradient based methods, the Canny detector is a convolution filter, but it is slightly more complicated and powerful. This method adopts a Gaussian mask as an optimal smoothing filter to eliminate the noise in an image while the other gradient based methods (especially, Sobel and Prewitt methods) use averaging filters (Adbel-Qader *et al.* 2003). The Gaussian G in a two-dimensional space is defined as

$$G = \exp\left(-\frac{x^2 + y^2}{2\sigma^2}\right) \quad (6)$$

where σ is the standard deviation.

After smoothing an image by the Gaussian filter, the Canny detector calculates the gradient modulus for each of X and Y directions and direction of the gradient at each pixel in the image. Central differential masks for the X and Y directions, Dx and Dy , are defined as (McAndrew 2004)

$$Dx = [-1 \ 0 \ 1], \quad Dy = [-1 \ 0 \ 1]^T \tag{7}$$

The gradient D and the direction θ_g at a pixel can be calculated as

$$D = \sqrt{(I_{sub} \bullet Dx)^2 + (I_{sub} \bullet Dy)^2}, \quad \theta_g = \tan^{-1} \left(\frac{I_{sub} \bullet Dy}{I_{sub} \bullet Dx} \right) \tag{8}$$

where I_{sub} is an arbitrary sub-image with 3×3 pixels in the image, and (\bullet) denotes a convolution operator. The convolution is the process of multiplying locationally similar entries and summing. For example, assuming 2 matrixes with 2×2 entries, the convolution of the matrixes is calculated by

$$\begin{bmatrix} a_1 & a_2 \\ a_3 & a_4 \end{bmatrix} \bullet \begin{bmatrix} b_1 & b_2 \\ b_3 & b_4 \end{bmatrix} = (a_1 \times b_1) + (a_2 \times b_2) + (a_3 \times b_3) + (a_4 \times b_4) \tag{9}$$

After the gradient calculations for all pixels in the image, non-maximum suppression, which is to find local maximum for the gradients, is applied for the pixels. Next, potential edges are detected again by using two thresholds, so called high threshold th_H and low threshold th_L . Noting that the other edge detectors use only one threshold and so use of the two thresholds is a unique characteristic of the Canny detector. If the gradient values for all pixels are larger than the high threshold, they are marked as strong edge pixels. If the gradient values for all pixels except the strong edge pixels are larger than the low threshold, they are marked as weak edge pixels.

Finally, the true edges are detected from tracking the potential edges by hysteresis. The strong edge pixels should be involved in the final edge image. If any of weak edge pixels is connected to the strong edge pixels, it is selected as a true edge. Otherwise, it is removed in the final edge image (Wikipedia).

2.3 Hough transform and circular Hough transform

2.3.1 Hough transform

The Hough transform (HT) is developed to find lines on an image by Hough (1959). The principle of the Hough transform is rather simple (McAndrew 2004). Supposing that (x, y) is a point in the image, a linear equation passing through the point can be written by $y=ax+b$. Then, all pairs (a, b) , which satisfy the equation, are estimated, and they are plotted into an “accumulator array” so called the “transform array”. Finally, if the highest values are found in the array, pairs (a, b) corresponding to them are selected as the strongest lines on the image.

Taking a binary image shown in Fig. 7(a) as an example, each point in the image is mapped onto a line in the transform, as shown in Fig. 7(b) (i.e., a point $(1, 0)$ is transformed as $b=-a$, indicated by the bold line on Fig. 7(b)). Two points $(1, 0)$ and $(1, -1)$ corresponding to the greatest number of intersections in the transform as plotted in Fig. 7(b) correspond to the strongest lines in the image. Therefore, the two strongest lines can written as $y=1$ and $y=-x-1$, as shown in Fig. 7(c). However, vertical lines cannot be expressed in the form of $y=ax+b$, so that another

parameterization of lines is used as

$$x \cos \theta + y \sin \theta = r \tag{10}$$

where r is the perpendicular distance from the line to the origin, and θ is the angle of the line's perpendicular to the x-axis, as shown in Fig. 8. In this parameterization, vertical lines are simply expressed to $\theta = 0$, and pairs (r, θ) are used to construct the transform array.

2.3.2 Circular Hough transform

The circular Hough transform (CHT) is an extended form of the HT to find circles in an image. The CHT is simpler than the HT, but it uses 3 parameters, center coordinates (c, d) of a circle, and the radius of the circle r_c while the HT uses only 2 parameters r and θ . In a two dimensional space, an equation of a circle is defined as (Duda and Hart 1971)

$$r_c^2 = (x - x_c)^2 + (y - y_c)^2 \tag{11}$$

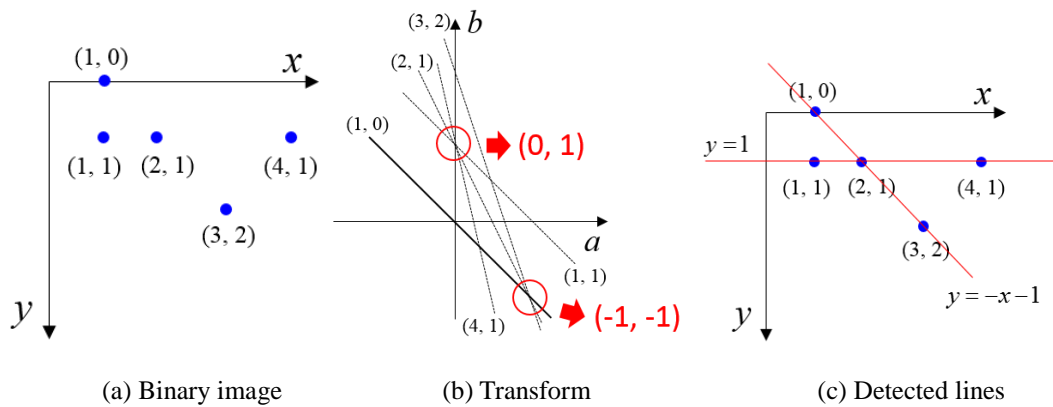


Fig. 7 Line detection on an image by using Hough transform (McAndrew 2004)

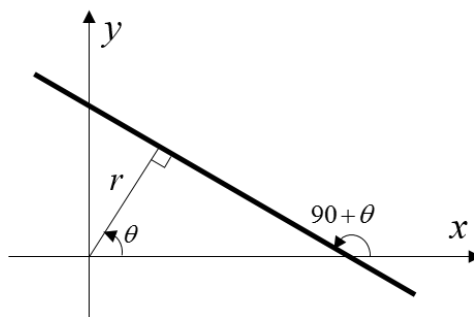


Fig. 8 A line expressed using $x \cos \theta + y \sin \theta = r$

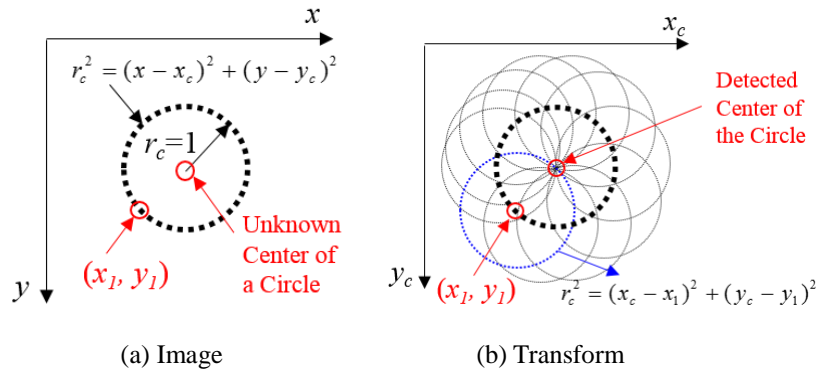


Fig. 9 An image and its corresponding circles in the transform

As shown in the Fig. 9(a), assume a circle with an arbitrary center point (x_c, y_c) and a known radius $r_c=1$. Substituting a point (x_1, y_1) on the circle into the Eq. (11), the equation is written as

$$r_c^2 = (x_c - x_1)^2 + (y_c - y_1)^2 \tag{12}$$

Eq. (12) represents a circle with the center point (x_1, y_1) and the radius $r_c=1$ in the transformed space with x_c and y_c axes. Circles in the transformed space corresponding to all pairs (x, y) can be plotted as shown in the Fig. 9(b). Similar to the HT process, the center coordinate (x_c, y_c) of the circle in the image is then obtained by searching the greatest number of intersections of the circles in the transformed space. For cases with unknown radius, the searching process should be repeated for all possible radius values. This searching job requires a larger computation time and memory of storage, so a specific range prior to running the application is set for simplicity.

3. Experimental evaluation on lab-scale bolted ring flange joint

3.1 Experimental setup

As the typical bolted connection in the steel WTT, a lab-scale bolted ring flange joint model was established to examine the applicability of the proposed vision-based technique for bolt-loosening monitoring. As shown in Fig. 10(a), the bolted joint model consists of a ring plate, bolts and nuts. The ring plate has an outer diameter of 52 cm, an inner diameter of 40 cm and a thickness of 1 cm. On the ring plate, 32 sets of standard bolt and nut, M20, were installed. Based on the labeling rule in Fig. 4, the bolts were numbered as shown in Fig. 10(a). The ring plate was painted by white color and the bolts and nuts were black-colored, as shown in Fig. 10(b). Note that the colors are commonly used in general steel WTTs.

A digital camera (D7000 model by Nikon Co. Ltd) with a lens (Tamron 17-50 mm f2.8) was used to take pictures of the bolted joint model. The camera was fixed on a tripod in front of the ring while the lens was set normal and heading to the center of the ring plate, see Fig. 11. The pictures were taken by using the maximum resolution (3253×4928 pixels) of the camera with sensor size of 23.5 × 15.6 mm. The photos were obtained by using an autofocus optical system of

the camera.

In order to practically determine the object distance (D), a 3 MW steel wind turbine operating in Jeju island of Korea was referred. The WTT is 77 m in height, assembled by 3 segments with 2 bolted ring flange joints. The largest outer diameter among the two bolted ring flanges is 3.462 m. A number of standard bolts and nuts, D42, were used to connect the steel tower segments. By using Eq. (1), the object distance (D) to picture all nuts of the bolted joint with the largest outer diameter was calculated as 3.773 m when the focal length is 17mm. If a picture is taken with an object distance of 3.8 m, a circular object with a diameter of 42 mm (i.e., the diameter of D42 bolt tip) will be projected to a size of 0.188 mm on the sensor of camera. Relating to the D20 bolt tip (the diameter of 20 mm) of the lab-scale test model, the object distance (D) should be set at 1.8 m to obtain the same size with the D42 bolt tip on the camera’s sensor (i.e., 0.188 mm), as explained below

$$D(m) : 20(\text{mm}) = 3.8(\text{m}) : 42(\text{mm}), \quad \therefore D = 1.8 \text{ m} \tag{13}$$

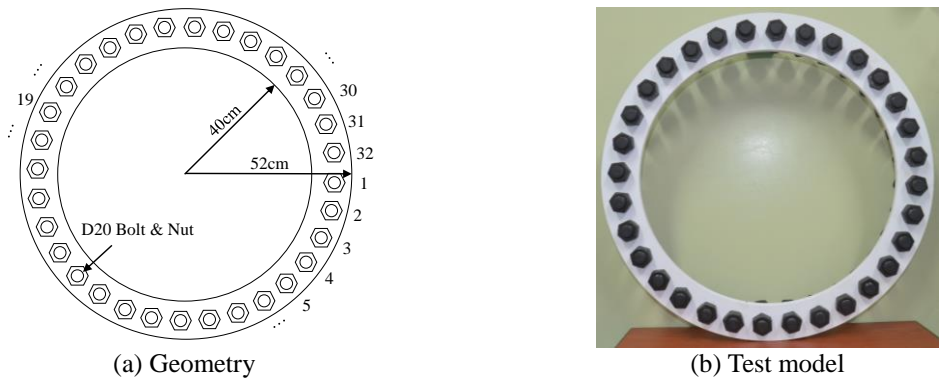


Fig. 10 A lab-scale bolted ring flange joint model

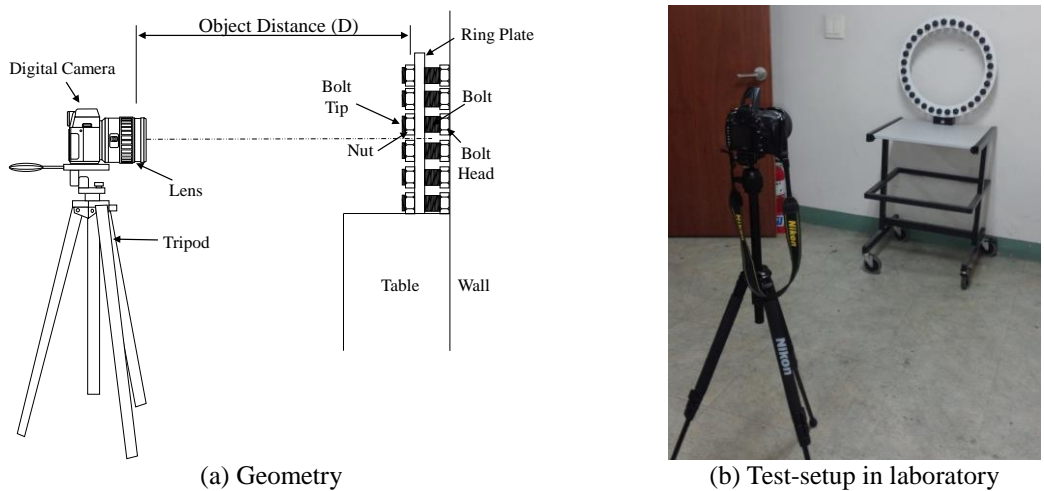


Fig. 11 Experimental setup of lab-scale bolted ring flange joint

Table 1 Bolt-loosening scenarios for the experimental evaluation of the proposed technique

Case	Loosened Bolt #	Nut's Angle Change ($\Delta\theta$)	Number of Pictures
Undamaged	-	-	11
Damage 1	4	-4	10
Damage 2	4	-27	10
Damage 3	4	-43	10
Damage 4	4	-49	10
	19	-7	
Damage 5	4	-53	10
	19	-19	

In order to evaluate the feasibility of the proposed bolt-loosening detection technique, several bolt-loosening scenarios were selected as listed in Table 1. While Damages 1~3 are single bolt-loosening cases, Damages 4~5 are two bolts-loosening cases. In Table 1, the change of the nut's angle ($\Delta\theta$) means the variation of the rotation angles of nuts measured by a goniometer before and after damage. It is assumed that the bolt-loosening is gradually progressed. A photo of the test model was firstly taken for the reference. To evaluate the accuracy of the proposed technique, 10 pictures were taken for each test scenario. Totally, 11 photos were captured for the undamaged case and 50 photos for the 5 damage cases. The images were shot with the resolution of 3253×4928 pixels, the focal lens of 17 mm, and the aperture of 2.8. It is noted that the camera's location was fixed during the testing process.

3.2 Bolt-loosening detection

3.2.1 Nuts' angle extraction

For detecting loosening occurrence in the bolted joint model, initial rotation angles of all nuts are needed as shown in Eq. (5). The initial angles were extracted from the first pictured image by Steps 1~4 of the proposed technique. Fig. 12 shows the full image of 3253×4928 pixels and the monitoring range of 1100×1100 pixels. The same monitoring range was used to remove extra objects, which may cause noises, for all pictured images.

Fig. 13(a) shows edges of the image detected by Step 2 of the proposed technique. The high and low thresholds for the Canny detector, which were determined from preliminary tests, were set at 0.04 and 0.08, respectively. The threshold values were ratios between target gradient thresholds and the maximum gradient in the image. As shown in the figure, all nuts and bolt tips were completely identified.

In Step 3, circular shapes in the image, which represents bolt tips, were firstly detected by using the CHT. The radius r_c used for the CHT, which was also determined from the preliminary tests, was ranging from 20 to 30 pixels. Blue colored circles in Fig. 13(b) indicates the identified bolt tips by the CHT. The image was then segmented for each nut by using center coordinates and radius of the detected circles as shown in Fig. 3. By setting $n = 1.7$ in Eq. (2), the sizes of segmented images were determined. The segmented images were automatically labeled from

Bolt#1 to Bolt#32, as shown in Fig. 13(b). All bolt tips were successfully identified and their labels were perfectly matched to the numbers in Fig. 10(a).

In Step 4, the sidelines of the nuts in the sub-images were identified using the HT. Before the HT was conducted, edge detection process by the Canny detector was repeated to remove noise on the each segmented image (e.g., shadow) and to clearly detect the edges of the nuts. In this step, the high and low thresholds of the Canny detector were set to 0.1 and 0.3, respectively. Fig. 14 shows the edges re-detected by the Canny detector for each sub-image. Compared with Fig. 13(a), the edges of the nuts were clearer and the edges by shadows as well as the bolt tips were removed. Then, the sidelines of the nuts were identified by the HT, as also shown in Fig. 14.



Fig. 12 Original image for initial condition and monitoring range for bolt-loosening detection of bolted joint

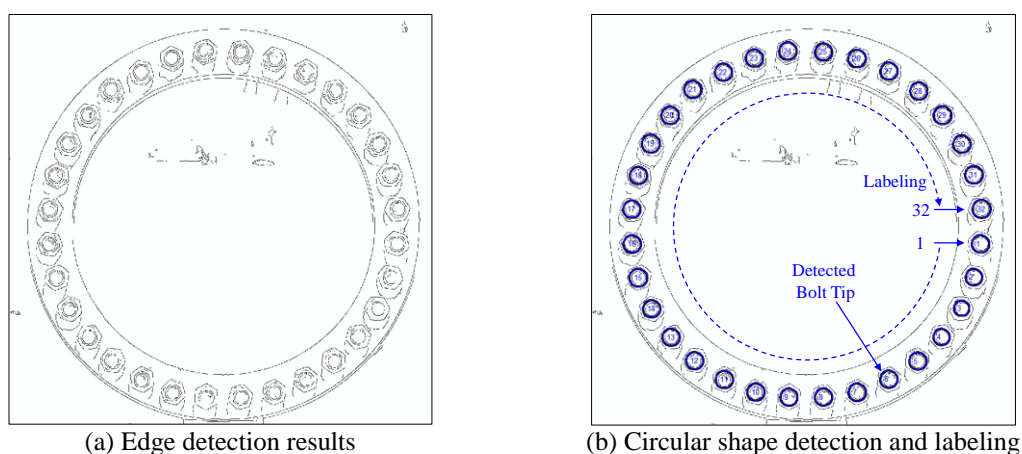


Fig. 13 Detected edge and circular shape detection and labeled nut images

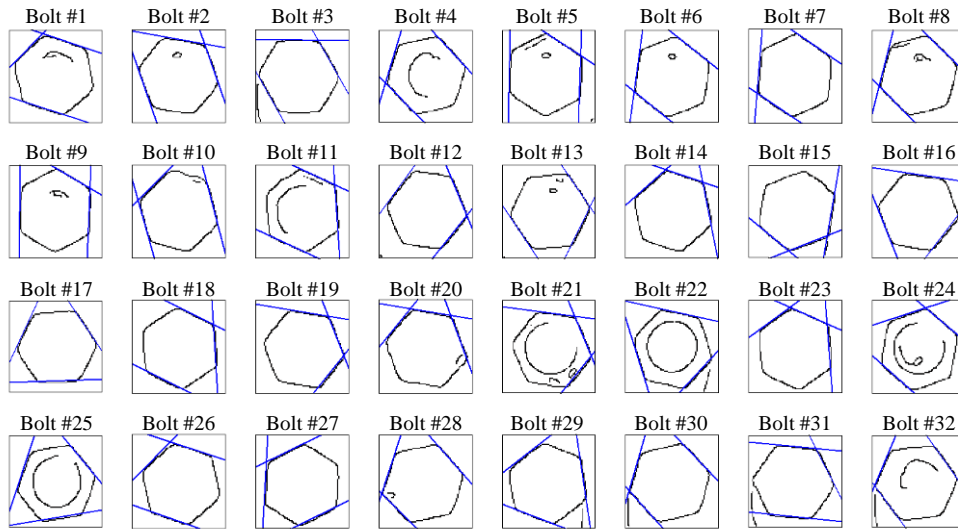


Fig. 14 Line detection results for each nut

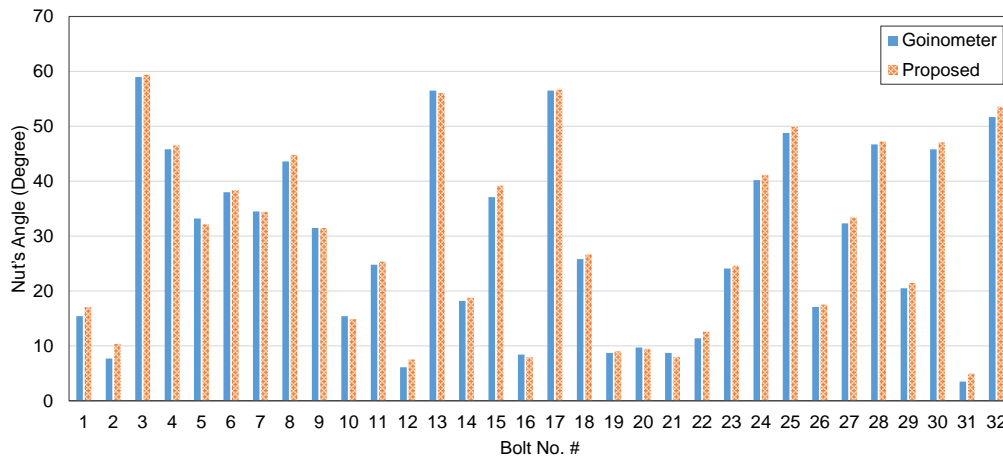


Fig. 15 Rotational angles of nuts estimated for initial image

Next, the rotation angles of the nuts were all computed using Eqs. (3) and (4). A comparison between the computed rotation angles and the measured ones by the goniometer was carried out, as plotted in Fig. 15. It is observed that the rotation angles obtained by the proposed technique and the goniometer were consistently matched for all bolts of the test connection. The maximum and minimum estimation errors of the vision-based technique were only 2.5 degrees and -1.1 degrees, respectively.

3.2.2 Decision-making on bolt-loosening

For bolt-loosening detection, the nuts' angles were extracted for all pictures captured from the undamaged and the damage cases. In order to deal with the uncertain conditions caused by experimental and computational errors, upper and lower limits were statistically established for decision-making on bolt-loosening. Firstly, the first pictured image in the undamaged case was set as the reference; and the loosened Bolts 4 and 19 in the damaged cases were excluded in the calculation.

Next, the consistency of the nut angle computation was examined by statistically analyzing the differences in angles estimated from the reference image and from the others. Totally, 1,800 samples (30 bolts \times 60 images) were used for the statistical analysis. Table 2 and Fig. 16 show the statistics for the consistency of the nut angle calculation and a histogram of the estimation errors. It is observed that the maximum and minimum differences were 2.5 degrees and -2.6 degrees, respectively. Also, the average difference was computed as 0.0 degree, and it means that the more pictures are used for the averaging, the higher accuracy is. From the statistical analysis, the lower and upper limits were set at -2.6 degrees and 2.6 degrees for the bolt-loosening monitoring by considering the minimum difference. For the selected limits, the confidence level was 99.987%.

As the final step, a control chart was constructed for decision-making on bolt-loosening monitoring, as shown in Fig. 16. The figure shows monitoring results for the loosened bolts (i.e., Bolt#4 and Bolt#19). It is noted that the other bolts could not be alarmed since the uncertain errors for constructing the upper and lower limits were evaluated from them. As shown in Fig. 16, all bolt-loosening cases were successfully alarmed, except 4 tests in Damage 1 (i.e., Tests 3, 6, 7 and 10). Table 3 shows the changes in nut angles of Bolt 4 and Bolt 19 estimated by the vision-based method and measured by the goniometer. As listed in the table, the rotation angles estimated in Damage 1 by the vision-based technique were ranging from -4.3 ~ -2.1 degrees, which was partially out of the control limit of -2.6 ~ 2.6 degrees. This false negative was caused by the estimation errors. When the mean values of the rotation angles were used for bolt-loosening detection, however, all damage scenarios were successfully alarmed, as observed in Table 3. It is also observed that the nut angle changes estimated by the vision-based method were well-matched with the ones measured by the goniometer. These experimental results proved the feasibility of the proposed vision-based technique for bolt-loosening detection in bolted joint of steel tower sections.

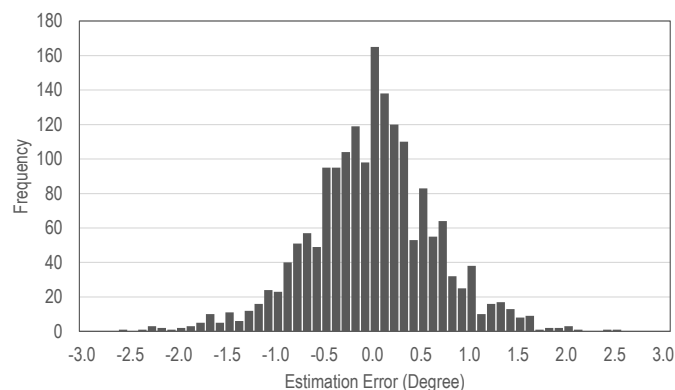


Fig. 16 Histogram of estimation errors

Table 2 Statistics for the consistency of the nut angle computation

Minimum	Maximum	Average	Standard Deviation
-2.6°	2.5°	0.0°	0.65°

Table 3 Bolt-loosening angles estimated by vision-based technique and measured by digital goniometer

Case	Loosened Bolt #	Measured $\Delta\theta$ (degree)	Estimated $\Delta\theta$ (degree)		
			Min	Max	Mean
Damage 1	4	-4	-4.3	-2.1	-3.0
Damage 2	4	-27	-28.3	-27.0	-27.6
Damage 3	4	-43	-42.3	-41.5	-42.1
Damage 4	4	-49	-42.8	-47.8	-48.7
	19	-7	-6.4	-5.7	-6.0
Damage 5	4	-53	-52.0	-50.1	-51.1
	19	-19	-18.1	-17.4	-17.8

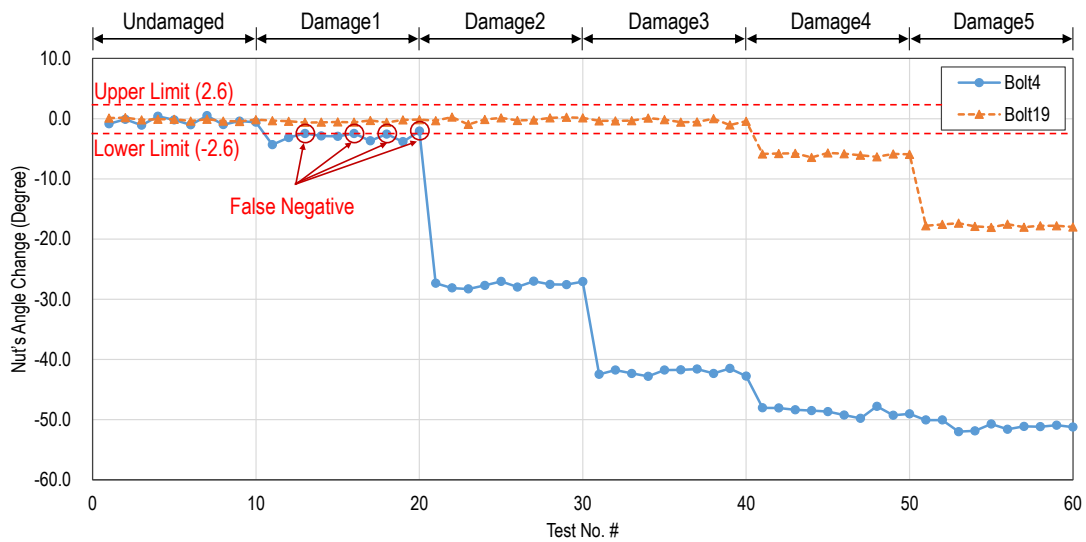


Fig. 17 Decision-making on bolt-loosening monitoring

4. Conclusions

In this study, a novel vision-based bolt-loosening monitoring technique was proposed for bolted joints connecting tubular steel segments of the WTT structure. Firstly, a bolt-loosening detection algorithm, which was based on image processing techniques, was developed. The algorithm consisted of acquiring an image for a bolt joint, locating all nuts in the image and segmenting the image for the each nut using the Canny edge detector and the circular Hough transform, identifying lines corresponding to outlines of the each nut by the Hough transform, estimating rotation angles of the each nut, and detecting bolt-loosening occurrence by the change of the rotation angles estimated from the reference and current images. Secondly, experimental tests were conducted on a lab-scale bolted joint model under various bolt-loosening scenarios. The bolted joint model, which was consisted of a ring flange and 32 sets of bolt and nut, was used for simulating the real bolted joint connecting steel tower segments in the WTT. Finally, the feasibility of the proposed vision-based technique was evaluated by bolt-loosening monitoring in the lab-scale bolted joint model. From the experimental results, the following conclusions have been made:

- The rotation angles of all nuts estimated by the vision-based technique were consistently matched to the ones measured by the goniometer with the errors ranging from -1.1 to 2.5 degrees.
- By investigating the consistency of the nut angle computation for all non-loosened nuts of all images, the accuracy of the vision-based technique was estimated within ± 2.6 degrees.
- The vision-based technique successfully alarmed all bolt-loosening tests, except several false-negatives were occurred for small severities of bolt-loosening. The method became more precise if the mean value of the rotation angles was used for decision-making.
- The proposed technique is promising for bolt-loosening detection in large-sized bolted joints of steel WTTs as well as steel bridges.
- If the perspective distortion by the angle of view of a camera is corrected, the proposed technique will be potential for the inspection of bolted joints in steel structures using portable cameras or drones.

This research preliminarily focused on verifying a new concept that uses vision images to detect bolt loosening in the wind turbine tower structure. As the future study, the proposed technique should be evaluated for the real structures. Also, the effect of the camera performances including perspective and radial distortions and environmental conditions such as brightness should be analyzed in details.

Acknowledgments

This work was supported by a Research Grant of Pukyong National University (2014 year). The graduate students and BK21plus professor involved in the research were also partially supported by the Brain Korea 21 Plus program of Korean Government.

References

- Abdel-Qader, I., Abudayyeh, O. and Kelly, M.E. (2003), "Analysis of edge-detection techniques for crack identification in bridges", *J. Comput. Civil Eng. - ASCE*, **17**(4), 255-263.
- Basava, S. and Hess, D.P. (1998), "Bolted joint clamping force variation due to axial vibration", *J. Sound Vib.*, **210**(2), 255-265.
- Canny, J.F. (1986), "A computational approach to edge detection", *IEEE T. Pattern Anal.*, **8**(6), 679-698.
- Choi, K.Y. and Kim, S.S. (2005), "Morphological analysis and classification of types of surface corrosion damage by digital image processing", *Corros. Sci.*, **47**(1), 1-15.
- Ciang, C.C., Lee, J.R. and Bang, H.J. (2008), "Structural health monitoring for wind turbine system: a review of damage detection methods", *Meas. Sci. Technol.*, **19**(12), 1-20.
- Fukuda, Y., Feng, M.Q., Narita, Y., Kaneko, S. and Tanaka, T. (2013), "Vision-based displacement sensor for monitoring dynamic response using robust object search algorithm", *IEEE Sensor J.*, **13**(12), 4725-4732.
- Ho, H.N., Kim, K.D., Park, Y.S. and Lee, J.J. (2013), "An efficient image-based damage detection for cable surface in cable-stayed bridges", *NDT&E Int.*, **58**, 18-23.
- Ho, H.N., Lee, J.H., Park, Y.S. and Lee, J.J. (2012), "A synchronized multipoint vision-based system for displacement measurement of civil infra structures", *The Scientific World J.*, **2012**, Article ID 519146, 1-9.
- Hough, P.V.C. (1959), "Machine analysis of bubble chamber pictures", *Proceedings of the 2nd International Conference on High-Energy Accelerations and Instrumentation*, Genova, Switzerland, September.
- Hutchinson, T.C. and Chen, Z. (2006), "Improved image analysis for evaluating concrete damage", *J. Comput. Civil Eng.*, **20**(3), 200-216.
- Huynh, T.C., Lee, K.S. and Kim, J.T. (2015), "Local dynamic characteristics of PZT impedance interface on tendon anchorage under prestress force variation", *Smart Struct. Syst.*, **15**(2), 375-393.
- Hyun, S.H. (2013), *The study on inspection for relaxation of bolted joins by electric potential drop method*, Master Dissertation, Chung-Ang University, Seoul.
- Izumi, S., Yokoyama, T., Iwasaki, A. and Sakai, S. (2005), "Threedimensional finite element analysis of tightening and loosening mechanism of threaded fastener", *Eng. Fail. Anal.*, **12**(4), 604-615.
- Kim, J.T., Park, J.H., Hong, D.S. and Ho, D.D. (2011), "Hybrid acceleration-impedance sensor nodes on Imote2-platform for damage monitoring in steel girder connections", *Smart Struct. Syst.*, **7**(5), 393-416.
- Kim, N. and Hong, M. (2009), "Measurement of axial stress using mode-converted ultrasound", *NDT & E Int.*, **42**(3), 164-169.
- Korea Expressway Corporation (2006), *Performance optimization of steel bridge coating diagnosing system for field application*, Research Report, Korea.
- Lee, S., Chang, L.M. and Skibniewski, M. (2006), "Automated recognition of surface defects using digital color image processing", *Automat. Constr.*, **15**(4), 540-549.
- McAndrew, A. (2004), *An introduction to digital image processing with matlab*, Course Technology Press, Boston, MA, USA.
- Park, G., Sohn, H., Farrar, C.R. and Inman, D.J. (2003), "Overview of piezoelectric impedance-based health monitoring and path forward", *Shock Vib. Digest*, **35**(6), 451-463.
- Park, S.H., Yun, C.B. and Roh, Y. (2006) "Active sensing-based real-time nondestructive evaluations for steel bridge members", *J. Civil Eng.- KSCE*, **10**(1), 33-39.
- Subirats, P., Dumoulin, J., Legeay, V. and Barba, D. (2006), "Automation of pavement surface crack detection using the continuous wavelet transform", *Proceeding of the 2006 IEEE International Conference on Image Processing*, Atlanta, USA, October.
- Wang, T., Song, G., Liu, S., Li, Y. and Xiao, H. (2013a), "Review of bolted connection monitoring", *Int. J. Distrib. Sens. N.*, **2013**, Article ID 871213, 1-8.
- Wang, T., Song, G., Wang, Z.G. and Li, Y.R. (2013b), "Proof-of-concept study of monitoring bolt connection status using a piezoelectric based active sensing method", *Smart Mater. Struct.*, **22**(8), Article

ID 087001.

Wikipedia, <https://en.wikipedia.org/>.

Yamaguchi, T. and Hashimoto, S. (2010), "Fast crack detection method for large-size concrete surface images using percolation-based image processing", *Mach. Vision Appl.*, **21**(5), 797-809.

You, Y.J., Park, K.T., Lee, W.S. and Han, S.H. (2010), "Development of information detection unit on the loosening of bolted joints using USN technology", *Proceeding of the Korea Society of Civil Engineers (KSCE) Conference & Expo 2010*, Incheon, Korea, October.

Zou, Q., Cao, Y., Li, Q., Mao, Q. and Wang, S. (2012), "CrackTree: automatic crack detection from pavement images", *Pattern Recogn. Lett.*, **33**(3), 227-238.